Journal of Advanced Ceramics https://mc03.manuscriptcentral.com/jacer

Journal of Advanced Ceramics
先进陶瓷
ISSN 2226-4108
CN 10-1154/TQ

J Adv Ceram 2026, **15**: 9221378

https://doi.org/10.26599/JAC.2026.9221378

Rapid Communication

Interfacial reaction-enabled strengthening of Al_2O_{3f}/Al_2O_3 composite joints brazed via TiO_2-modified Ag-Nb_2O_5 fillers

Chen Wang[1], Guiwu Liu[1,*], Qinhan Guo[1,2], Huan Liu[1], Xiangzhao Zhang[1,*] , Guanjun Qiao[1]

[1] *School of Materials Science and Engineering, Jiangsu University, Zhenjiang 212013, China*

[2] *School of Mechanical and Electrical Engineering, Taizhou University, Taizhou 225300, China*

* Corresponding authors.

E-mail: G. Liu, gwliu76@ujs.edu.cn;

X. Zhang, xzzhang2018@ujs.edu.cn

Received: July 24, 2026; Revised: August 31, 2026; Accepted: September 9, 2026

Abstract: Alumina fiber-reinforced alumina ceramic matrix composites (Al_2O_{3f}/Al_2O_3 CMCs) are strategic for extreme-environment applications, motivating the development of compatible joining methods. In this work, the reactive air brazing (RAB) of Al_2O_{3f}/Al_2O_3 CMC using Ag-4Nb_2O_5-$x$$TiO_2$ ($0 \leq x \leq 4$, in mol%) fillers was performed, and the microstructure evolution, interfacial behavior, and mechanical properties of brazed joints were systematically investigated. The main interfacial reaction product evolves from $AgNbO_3$ to $AlNbO_4$ with the TiO_2 content increasing, while the Ag interlayer gradually becomes discontinuous. When brazed with Ag-4Nb_2O_5-2TiO_2, the CMC/Al_2O_3 butt joint exhibits higher average shear strength (45.3 MPa) among the joints tested, outperforming the CMC/CMC butt joint, CMC/CMC flat joint, and CMC/GH3536 butt joint, with shear strengths of 38.1, 7.6, and 27.7 MPa. The fracture behavior of these joints is governed by multiple factors, namely interfacial features (the $AlNbO_4$ reaction layer, interlocking structure, and pores) and elemental diffusion from GH3536 alloy.

Keywords: Al_2O_{3f}/Al_2O_3 composites; Reactive air brazing; Microstructures; Interfaces; Mechanical properties.

1 Introduction

Alumina fiber-reinforced alumina ceramic matrix composites (Al_2O_{3f}/Al_2O_3 CMCs) offer excellent resistance to high temperatures, oxidation, thermal shock, and corrosion, combined with low density [1,2]. These characteristics render them capable of withstanding demanding conditions, which makes them important thermal structural materials for modern high-end equipment manufacturing in sectors such as aviation, aerospace, energy, and the chemical engineering. A notable application is in aviation engines, which encompass components including firewalls, combustion chamber outer bushings, center cones, mixers, and fairings [3,4]. The joining of these materials is therefore of significant importance to advancing material integration technologies in these fields. The joining of Al_2O_{3f}/oxide CMCs is key for the fabrication of corresponding composite components. The feasibility of active metal brazing (AMB) and glass-ceramic joining has been demonstrated by Malinverni et al. [5] and Akram et al. [6], respectively. In practice, both joining techniques have inherent limitations. The AMB process demands a protective atmosphere or high vacuum, inevitably introducing complexity and inconvenience. In contrast, glass-ceramic joints are typically characterized by inferior high-temperature strength and thermal shock resistance, which stem from the inherent brittleness of the glass-ceramic and its weak interfacial reactivity [7].

Reactive air brazing (RAB) is a joining technique that enables the bonding of ceramics to ceramics or to metals in air or oxidizing atmospheres. RAB fillers typically are composed of a precious metal (e.g., Ag, Pt) and metal oxides, resulting in joints with good high-temperature and oxidation resistances. To date, the RAB fillers of Al_2O_3 ceramics mainly consist of Ag-CuO system, Ag-SiO_2, and Ag-Nb_2O_5 [8,9]. Indeed, Ag-CuO-based fillers struggle to withstand high-temperature reducing atmospheres over extended periods [10], while Ag-SiO_2-based fillers yield joints with relatively low strength [11]. In contrast, the Ag-Nb_2O_5 brazing filler may produce high-temperature-resistant joints in both oxidizing and reducing atmospheres without compromising joint strength. Furthermore, the addition of a certain amounts of TiO_2 or Ti into Ag-8CuO filler can significantly enhance the wettability and joint strength with Al_2O_3 ceramics [12,13]. Thus, whether the addition of a certain amount of TiO_2 to the Ag-Nb_2O_5 system also yields beneficial effects remains an open question. In fact, the design principle of this filler system primarily consists of two aspects: (i) enhancing interfacial infiltration and favorable interfacial reactions, or suppressing unfavorable ones, and (ii) alleviating interfacial residual thermal stress by lowering the mismatch of coefficient of thermal expansion (CTE).

In this study, a certain amount (0–4 mol%) of TiO_2 was added to the Ag-4Nb_2O_5 filler to form composite fillers, in which the Ag-4Nb_2O_5 composition was chosen because it yielded the maximum joint strength in the previous studies [14,15]. For the first time, the Al_2O_{3f}/Al_2O_3 CMC was brazed to the 99% Al_2O_3 ceramic, itself and GH3536 in air, respectively. The cross-sectional microstructures, interfacial behavior, shear strength and fracture of the joints were mainly investigated. This study provides a viable joining strategy for Al_2O_{3f}/Al_2O_3 CMCs and demonstrates the beneficial effect of adding TiO_2 to the Ag-Nb_2O_5 brazing filler on joint strength.

2 Materials and methods

The 2D woven Al_2O_{3f}/Al_2O_3 CMCs (fiber volume fraction: 38%–45%; porosity: 23%–30%) were cut into substrates of 21 mm × 11 mm × 5 mm and 11 mm × 11 mm × 3 mm for butt and flat brazing, respectively. 99% Al_2O_3 ceramic plates and GH3536 nickel-based superalloy (both 23 mm × 13 mm × 5 mm) were used as substrates for butt brazing with the Al_2O_{3f}/Al_2O_3 CMC, respectively. Prior to brazing, the ceramic plates and GH3536 superalloy were cleaned in hot alkaline solution, polished with 400–1600 grit diamond discs, and ultrasonically rinsed in acetone and ethanol for 20 min each. Brazing fillers were prepared from Ag powders (~5 μm, 99.99%), Nb_2O_5 powders (~5 μm, 99.5%), and TiO_2 powders (~5 μm, 99%). The three powders were ball-milled in ethanol at 60 r/min for 48 h to prepare six brazing fillers with the nominal composition of Ag-4Nb_2O_5-$x$$TiO_2$ (x = 0, 0.5, 1, 2, 3, 4, in mol%). The six mixed powders were then dried, ground, compacted and cut into sheets of approximately 23 mm × 13 mm × 100 μm for RAB testing.

Figure S1(a) shows the schematic diagrams of the four brazing assemblies and the corresponding post-cut brazed joints. A ~100 μm thick Ag-4Nb_2O_5-$x$$TiO_2$ sheet was sandwiched either between the CMC plate and Al_2O_3 ceramic plate, between the CMC plate and another CMC plate, or between the CMC plate and the superalloy plate. The assembly was loaded with ~30 kPa and heated in a Nabertherm muffle furnace to 1150 °C at 5 °C/min. After holding at 1150 °C for 30 min, the specimen was cooled to 500 °C at 5 °C/min and then furnace-cooled to room temperature. The formed joints were cut into rectangular blocks of ~10 mm × 10 mm × 5 mm or ~11 mm × 6 mm × 5 mm. The resulting joints were tested in shear at a loading speed of 0.5 mm/min on a DDL100 universal testing machine (DOLI, Germany) equipped with a fixture (Fig. S1(b)). The shear strength values were averaged from 3–4 joint samples.

The cross-sectional microstructures of brazed joints were observed by scanning electron microscope (SEM). Phase identification on the joint cross-sections and fracture surfaces was performed using X-ray diffraction (XRD) and energy-dispersive spectrometer (EDS). The interface sample was observed and analyzed by transmission electron microscopy (TEM) coupled with EDS.

3 Results and discussion

Figure 1 presents the cross-sectional SEM micrographs of the CMC/Ag-4Nb_2O_5-$x$$TiO_2$/$Al_2O_3$ butt joints, CMC/CMC butt joint, CMC/CMC flat joint, and CMC/GH3536 butt joint. Table S1 summarizes the elemental compositions and possible phases of the characteristic microstructures in Figs. 1(a) and S2(a). As shown in Fig. 1(a), the interlayer of CMC/Ag-4Nb_2O_5/Al_2O_3 joint consists primarily of an Ag layer, while a small amount of gray $AgNbO_3$ is dispersed within the pores of the Al_2O_{3f}/Al_2O_3 CMC via capillary action driven by the liquid Ag. The $AgNbO_3$ forms via the reaction of Nb_2O_5 with Ag and O_2 [16,17], as described by Eq. 1.

$$4Ag + 2Nb_2O_5 + O_2 = 4AgNbO_3 \quad (1)$$

As shown in Figs. 1(a)–1(d), after the introduction of TiO_2, a dark gray reaction layer appears at the CMC/Ag interface, and this reaction layer gradually accumulates and becomes continuous as the TiO_2 content increases. To better observe this dark gray phase, a thin lamella containing the interfacial reaction layer was extracted from the Ag-4Nb_2O_5-2TiO_2/Al_2O_3 couple using focused ion beam (FIB) and then subjected to TEM analysis. As shown in Figs. 2(a) and 2(b), the interface region can be divided into two distinct phases, demarcated by the red dashed line. Based on these spacings and the SAED patterns, the two phases are identified as Al_2O_3 and $AlNbO_4$ (Figs. 2(c)–2(f)). In fact, the dark gray phase is confirmed to be a Ti-bearing $AlNbO_4$ solid solution phase according to the EDS result (Fig. 2(b)). The $AlNbO_4$ forms via the reaction of Nb_2O_5 with Al_2O_3 at ~1000 °C [18,19], as described by Eq. 2:

$$Al_2O_3 + Nb_2O_5 = 2AlNbO_4 \quad (2)$$

In fact, the addition of TiO_2 in Ag-based brazing fillers may cause partial dissolution of the Al_2O_3 substrate [20], leading to preferential reaction of Nb_2O_5 with the Al_2O_3 substrate to form an $AlNbO_4$ interfacial layer [21]. Consequently, this consumption of Nb_2O_5 inhibits the formation of $AgNbO_3$.

Based on the above TEM analysis and the EDS results (Table S1), the gray, dark gray, bright, and dark phases in CMC/Ag-4Nb_2O_5-$x$$TiO_2$/$Al_2O_3$ joint sections can be identified as $AgNbO_3$, $AlNbO_4$, Ag and Al_2O_3, respectively. Upon addition of 2 mol% TiO_2, a nearly continuous $AlNbO_4$ reaction layer forms at the interface, while a small amount of $AlNbO_4$ also appears near the Al_2O_3 ceramic substrate

(Fig. 1(d)). The preferential formation of $AlNbO_4$ at the CMC/Ag interface can be mainly attributed to higher activity of the Al_2O_3 fibers in the CMC substrate compared with the 99% Al_2O_3 ceramic substrate. At 3 mol% TiO_2, more $AlNbO_4$ forms at both the Ag/CMC and Ag/Al_2O_3 interfaces, and this phase partially enters the Ag interlayer, resulting in a locally discontinuous Ag interlayer (Fig. 1(e)), which can severely impair the mechanical strength of the joint. At 4 mol% TiO_2, much more $AlNbO_4$ is produced between the two substrates, leading to the disappearance of the continuous Ag layer (Fig. 1(f)). The massive accumulation of the brittle $AlNbO_4$ phase throughout the interlayer, together with the loss of the continuous Ag layer due to excessive interfacial reaction, directly embrittles the joint and further reduces the joint shear strength.

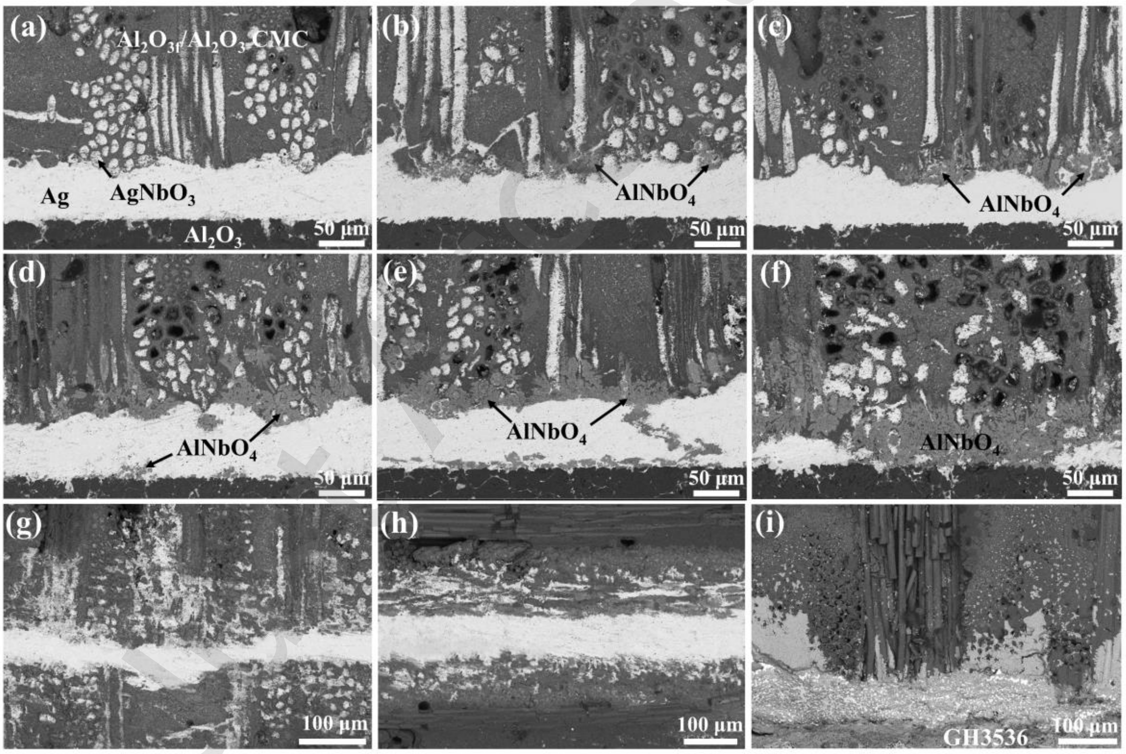

Fig. 1 Cross-sectional SEM micrographs of (a–f) CMC/Ag-4Nb_2O_5-$x$$TiO_2$/$Al_2O_3$ butt joints (x=0, 0.5, 1, 2, 3, and 4), and (g) CMC/CMC butt, (h) CMC/CMC flat, and (i) CMC/GH3536 butt joints brazed using Ag-4Nb_2O_5-2TiO_2.

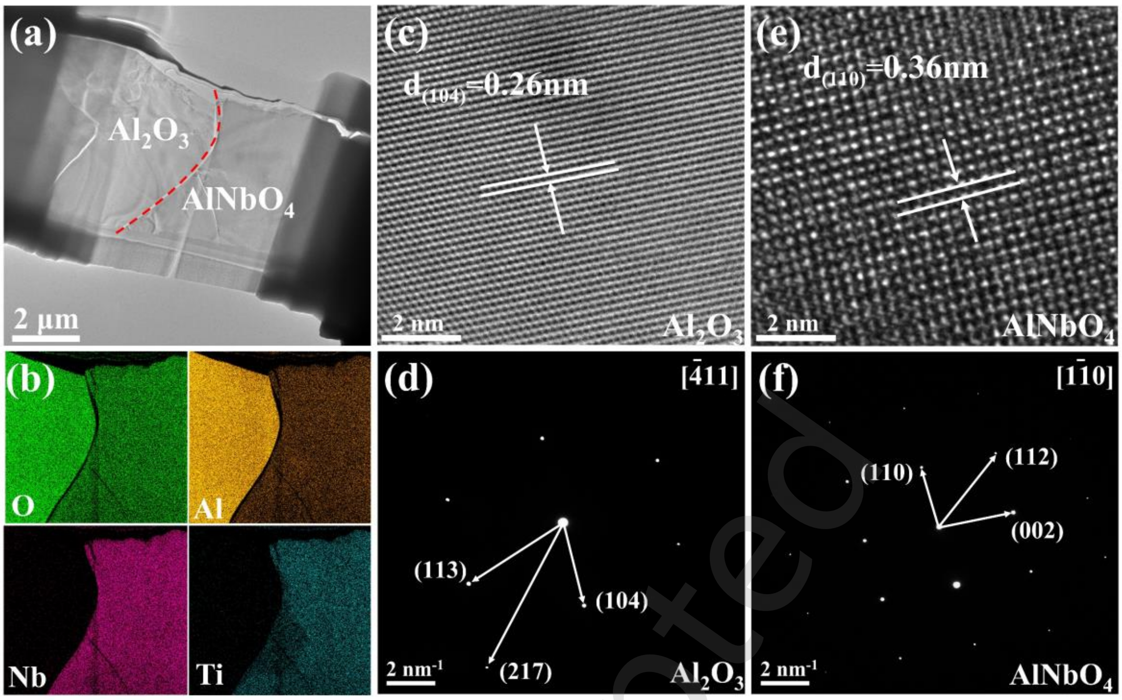

Fig. 2 (a) TEM image, (b) EDS elemental maps, (c, d) HRTEM images, and (e, f) the corresponding SAED patterns of Ag-4Nb_2O_5-2TiO_2/Al_2O_3 interface.

Figure 3(a) illustrates the variation in average shear strength of the CMC/Ag-4Nb_2O_5-$x$$TiO_2$/$Al_2O_3$ joint as a function of TiO_2 content. The joint shear strength first increases and then decreases with the TiO_2 content increasing from 0 to 4 mol%, peaking at 45.3 MPa at 2 mol%. With increasing TiO_2 addition in the CMC/Ag-4Nb_2O_5/Al_2O_3 system, the $AlNbO_4$ reaction layer evolves systematically from absence, to discontinuous adhesion, to continuous adhesion, and finally to penetration through the Ag interlayer with the formation of block-like structures. This microstructure evolution exerts a decisive influence on the joint mechanical properties. Specifically, an insufficient $AlNbO_4$ layer leaves Ag in direct contact with both substrates, resulting in weak interfacial bonding. A relatively continuous layer, on the other hand, effectively accommodates the CTE mismatch, thereby enhancing joint strength. However, excessive formation of $AlNbO_4$ leads to penetration across the interlayer, inducing stress concentration and consequently degrading the mechanical properties.

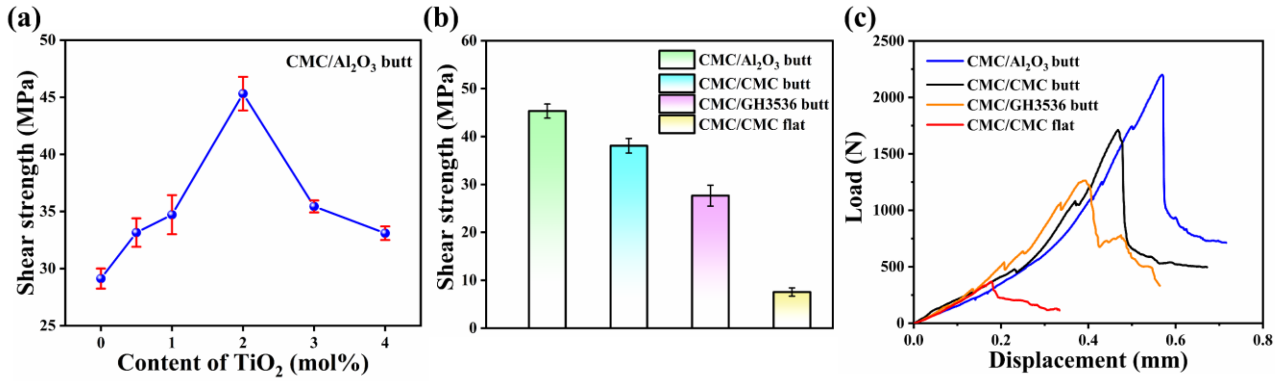

Fig. 3 (a) Variation of average shear strength of CMC/Ag-4Nb_2O_5-$x$$TiO_2$/$Al_2O_3$ butt joints with TiO_2 content. (b) Joint shear strength of CMC/Al_2O_3 butt, CMC/CMC butt, CMC/GH3536 butt, and CMC/CMC flat joints brazed with Ag-4Nb_2O_5-2TiO_2, and (c) the corresponding load-displacement curves.

To further investigate the potential application of the Ag-4Nb_2O_5-2TiO_2 brazing filler for joining the Al_2O_{3f}/Al_2O_3 CMC, the other three types of joints were brazed: CMC/CMC butt joint, CMC/CMC flat joint, and CMC/GH3536 butt joint. As shown in Figs. 3(b) and 3(c), the shear strengths of CMC butt joints to different substrates are significantly higher than that of CMC/CMC flat joints (7.6 MPa), which may be closely related to uneven brazing surface of CMC substrate. During the brazing of butt joints, capillary action enables the molten Ag to infiltrate the micropores of the CMC substrate, resulting in an interlocking structure between the filler and the substrate (Fig. 1(g)), which is beneficial for relieving the residual stress at the interface. However, in flat joints, many pores are generated at the interface due to the uneven surface of CMC substrate (Fig. 1(h)). Furthermore, the average shear strength (27.7 MPa) of CMC/GH3536 butt joint is lower than those of CMC/Al_2O_3 and CMC/CMC butt joints (45.3 and 38.1 MPa), which is mainly attributed to huge residual thermal stress originated from the greater difference in CTE between the CMC substrate and the GH3536 Ni-based superalloy. The CTE values of the Al_2O_{3f}/Al_2O_3 CMC, 99% Al_2O_3 ceramic, and GH3536 are approximately 6.04×10^{-6}–8.04×10^{-6} K^{-1} [22], 8.2×10^{-6} K^{-1} [23], and 13×10^{-6} K^{-1} [24], respectively. As shown in Fig. 1(i), the interlayer of the CMC/GH3536 butt joint is considerably disordered. This is attributed to the extensive interdiffusion of Ni, Cr, and Fe from the GH3536 alloy into the Ag layer (Table S2), which ultimately prevents the formation of a continuous Ag layer.

Figures 4(a)–4(d) present the macroscopic photograph, microstructural morphologies, and XRD pattern of the fracture surface from a typical CMC/Ag-4Nb_2O_5-2TiO_2/Al_2O_3 joint, while Figures 4(e)–4(h) show schematic fracture paths for the four kinds of brazed joints. Based on the macro and micro images of fracture surface and the identified phase composition, the final fracture of this joint primarily occurs in the CMC substrate, which is designated as CMC fracture. The fracture exhibits a mixed mode, characterized by both brittle fracture and ductile behavior, and it is in good agreement with the load-displacement curves in Fig. 3(c). Indeed, a small amount of discrete $AgNbO_3$ phase is present between the $AlNbO_4$ layer and the CMC substrate (Fig. 4(b)), which only has a very limited impact on the mechanical properties of the joint. During shear testing, the crack initiates at the interface near the Al_2O_3 substrate, propagates through the interlayer, and finally terminates within the CMC substrate (Figs. 4(a) and 4(e)), thus demonstrating higher joint shear strength. However, the CMC/CMC butt joints mainly fail at the discontinuous interfacial reaction layer (referred to as reaction layer fracture), with one exception occurring within the CMC substrate (Fig. 4(f)). Furthermore, the fracture of the CMC/GH3536 butt joint occurs mainly within the interlayer (i.e., interlayer fracture), which is attributed to extensive elemental diffusion from the GH3536 alloy into the Ag layer during brazing (Fig. 4(g)). In the CMC/CMC flat joint, fracture takes place at the interface on one side of the substrate (i.e., interfacial fracture) (Fig. 4(h)), owing to the absence of an interlocking structure and the presence of numerous interfacial pores, which results in the lowest joint shear strength. Therefore, multiple factors govern the fracture behavior of these joints, including interfacial features (the $AlNbO_4$ reaction layer, interlocking structure, and pores) and elemental diffusion from the GH3536 alloy.

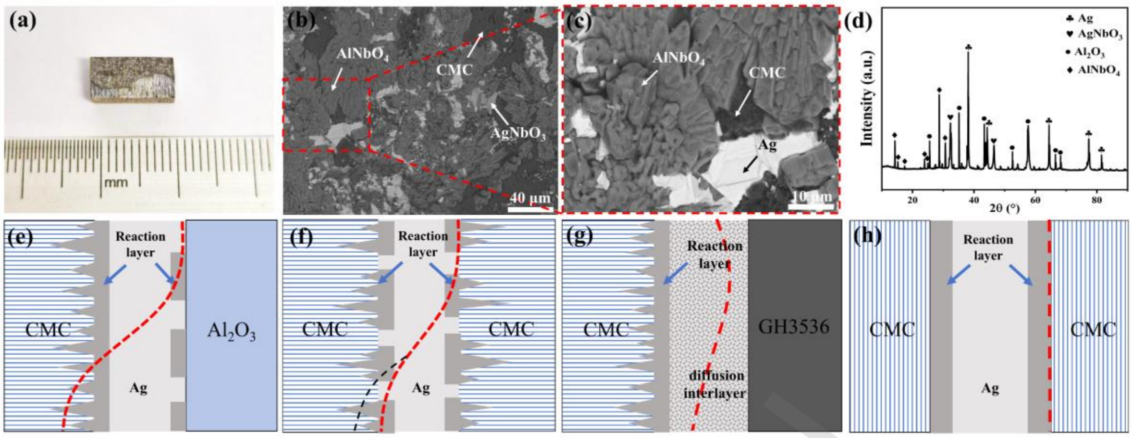

Fig. 4 (a) Macroscopic photograph, (b, c) microstructural morphologies, and (d) XRD pattern of fracture surface from a typical CMC/Ag-4Nb_2O_5-2TiO_2/Al_2O_3 joint. Schematic fracture paths for the (e) CMC/Al_2O_3 butt, (f) CMC/CMC butt, (g) CMC/GH3536 butt, and (h) CMC/CMC flat joints.

4 Conclusions

Using Ag-4Nb_2O_5-2TiO_2 filler, Al_2O_{3f}/Al_2O_3 CMC was successfully brazed to 99% Al_2O_3 ceramic, itself, and GH3536 alloy in air. The CMC/Al_2O_3 butt joint exhibits the highest average shear strength of 45.3 MPa, followed by the CMC/CMC butt joint, CMC/GH3536 butt joint, and CMC/CMC flat joint. The addition of TiO_2 promotes the formation of $AlNbO_4$ via the interfacial reaction between Nb_2O_5 and Al_2O_3, which consequently consumes the Nb_2O_5 and inhibits the formation of $AgNbO_3$, leading to a progressive evolution of the $AlNbO_4$ layer from absence, to discontinuous adhesion, to continuous adhesion, and ultimately to penetration through the Ag interlayer as block-like aggregates. At 2 mol% TiO_2, a nearly continuous $AlNbO_4$ layer forms at Ag/CMC interface, while the infiltration of Ag together with reaction products ($AgNbO_3$ and $AlNbO_4$) into the CMC substrate, creating an interlocking structure that enhances joint strength. The fracture behavior of these joints is thus controlled by both interfacial features (the $AlNbO_4$ layer, interlocking structure, and pores) and elemental diffusion from GH3536.

Acknowledgements

This work is supported by National Natural Science Foundation of China (52572073, 52002153), Natural Science Research Project of the Jiangsu Higher Education Institutions (25KJA460010), Taizhou Natural Science Foundation General Program (TZ202512), and Taizhou Science and Technology Support Plan Project (TS202403).

Author contributions

Chen Wang: Investigation, Methodology, Visualization, Writing – original draft. Guiwu Liu: Formal analysis, Visualization, Writing – review & editing, Resources, Supervision. Qinhan Guo: Conceptualization, Methodology. Huan Liu: Methodology, Visualization. Xiangzhao Zhang: Conceptualization, Formal analysis, Visualization. Guanjun Qiao: Resources, Funding acquisition.

Availability of data and materials

The data that support the findings of this study are available from the corresponding author upon reasonable request.

Competing interests

The authors have no competing interests to declare that are relevant to the content of this article. The author Guiwu Liu is the Editorial Committee member of this journal.

Electronic Supplementary Material (ESM)

Electronic Supplementary Material is available in the online version of this article

References

[1] Xu T, Li G, Fan Z, *et al*. High-temperature tensile behavior and failure mechanism of 2D woven Al_2O_{3f}/Al_2O_3 composites with multiscale study. *J Eur Ceram Soc* 2026, **46**: 118500.

[2] Jiang Y, Xu R, Jiang R, *et al*. High-temperature mechanical properties and thermal shock resistance of an alumina-fiber-reinforced alumina ceramic matrix composite. *Ceram Int* 2025, **51**: 5459–5469.

[3] Liu Q, Liang Y, Qiu H, *et al*. Research progress on continuous alumina fibers and its composite material. *Adv Ceram* 2024, **45**: 385–407.

[4] Liang YY, Jin JY, Yan J, *et al*. Preparation and properties of Al_2O_{3f}/Al_2O_3-SiC ceramic matrix composite. *Adv Ceram* 2025, **46**: 377–388.

[5] Malinverni C, Casalegno V, Bertrand P, *et al*. Titanium-based brazing alloy for bonding oxide/oxide CMCs for steelmaking industry applications. *J Eur Ceram Soc* 2025, **45**: 117231.

[6] Akram MY, Ferraris M, Casalegno V, *et al*. Joining and testing of alumina fibre reinforced YAG-ZrO_2 matrix composites. *J Eur Ceram Soc* 2018, **38**: 1802–1811.

[7] Guo Q, Xu S, Zhang X, Gui X, *et al*. Microstructures and interfacial behavior of Ag-CuO/AlN system by air wetting and brazing: Experiments and first-principles calculations. *J Eur Ceram Soc* 2024, **44**: 4963–4974.

[8] Zhang M, Xu S, Valenza F, Zhang X, *et al*. Advances in reactive air wetting and brazing of engineering ceramics. *J Adv Ceram* 2025, **14**: 9220997.

[9] Si X, Wang X, Guo X, *et al*. Review of reactive air brazing: fundamental, progress, and perspective. *Mater Des* 2024, **243**: 113073.

[10] Kim JY, Hardy JS, Weil KS. High-temperature tolerance of the silver-copper oxide braze in reducing and oxidizing atmospheres. *J Mater Res* 2006, **21**: 1434–1442.

[11] Wang Z, Li C, Si X, *et al*. Microstructure and mechanical properties of Al_2O_3 ceramic joints achieved by Ag-SiO_2 braze in air. *Int J Appl Ceram Technol* 2022, **19**: 508–513.

[12] Zhang M, Guo Q, Zhang Y, *et al*. The role of TiO_2 in modifying Ag-8CuO for reactive air wetting and brazing of Al_2O_3: Microstructure evolution and mechanical properties. *Ceram Int* 2026, **52** 9325–9332.

[13] Bobzin K, Schlaefer T, Zhao L, *et al*. Brazing of ceramic-to-ceramic and ceramic-to-metal joints in air. *Front Mech Eng China* 2010, **5**: 125–129.

[14] Zhang X, Zhang Y, Wang C, *et al*. Enhanced Ag-Nb_2O_5/SiC wetting and brazing by SiC pre-oxidation: Experiments and first-principles study. *J Am Ceram Soc* 2026, **109**: e70360.

[15] Qiu Y, Xu S, Zhang X, *et al*. Reactive air wetting and brazing of Al_2O_3 ceramics using Ag-Nb_2O_5 filler: Performance and interfacial behavior. *J Adv Ceram* 2024, **13**: 135–142.

[16] Zhang M, Carstensen L, Zhao C, *et al*. Revealing the solid-state processing mechanisms of antiferroelectric $AgNbO_3$ for energy storage. *J Am Ceram Soc* 2022, **105**: 451–460.

[17] Valant M, Axelsson A, Zou B, *et al*. Oxygen transport during formation and decomposition of

$AgNbO_3$ and $AgTaO_3$. *J Mater Res* 2007, **22**: 1650–1655.

[18] Chen J, Chen Q, Qu SJ, *et al*. Oxidation mechanisms of an intermetallic alloy at high temperatures. *Scr Mater* 2021, **199**:113852.

[19] Gu J, Pan L, Yang J, *et al*. Mechanical properties and oxidation behavior of Ti-doped Nb_4AlC_3. *J Eur Ceram Soc* 2016, **36**: 1001–1008.

[20] Weil KS, Kim JY, Hardy JS, *et al*. The effect of TiO_2 on the wetting behavior of silver-copper oxide braze filler metals. *Scr Mater* 2006, **54**: 1071–1075.

[21] Guo Q, Zhang M, Zhang X, *et al*. Interfacial behavior and joint mechanical properties of Ag/AlN system: The role of Nb_2O_5 addition. *Ceram Int* 2026, **52**: 20073–20081.

[22] Wang P, Liu X, Wang H, et al. Releasing the residual stress of C_f/SiC-GH3536 joint by designing an Ag-Cu-Ti + $Sc_2(WO_4)_3$ composite filler metal. *J Mater Sci Technol* 2022, **108**: 102–109.

[23] Liu Q, Pang B, Liang Y, et al. Effect of reinforcement structure on Al_2O_3/Al_2O_3 composite properties. *Aeronaut Manuf Technol* 2026, **69**: 25020327.

[24] Tillmann W, Anar NB, Wojarski L. Mechanical behavior of reactive air brazed (RAB) Crofer 22 APU–Al_2O_3 joints at ambient temperature. *SN Appl Sci* 2020, **2**: 809.